Biomaterials and Biosystems 21 (2026) 100126

Contents lists available at ScienceDirect

Biomaterials and Biosystems

journal homepage: www.elsevier.com/locate/bbiosy

Durable and biofunctional polydimethylsiloxane surfaces engineered with photocrosslinkable terpolymers for aligned and functional myotube formation

Ryoma Takagi [a,b], Tadashi Nakaji-Hirabayashi [a,b,c,d,*], Moe Kato [a,b], Miwako Shobo [a], Chiaki Yoshikawa [a,*]

[a] Research Center for Macromolecules and Biomaterials, National Institute for Materials Science, Ibaraki 305-0047, Japan
[b] Graduate School of Innovative Life Science, University of Toyama, 3190 Gofuku, Toyama 930-8555, Japan
[c] Graduate School of Science and Engineering, University of Toyama, 3190 Gofuku, Toyama 930-8555, Japan
[d] Faculty of Engineering, Academic Assembly, University of Toyama, 3190 Gofuku, Toyama 930-8555, Japan

ARTICLE INFO

Keywords:
Polydimethylsiloxane surface modification
Photocrosslinkable polymer coating
Bioinert–bioactive interface
Collagen-functionalized surface
Myoblast differentiation and alignment
Microstructured substrate
Muscle tissue engineering

ABSTRACT

Polydimethylsiloxane (PDMS) is widely used in biomicrodevices owing to its excellent processability, flexibility, and optical properties. However, the poor cell adhesiveness of PDMS limits its application as a stable substrate for long-term cell cultures. To address these challenges, we synthesized a photocrosslinkable terpolymer composed of *N*-(2-hydroxypropyl)acrylamide, *N*-benzophenone acrylamide, and *N*-succinimidyl acrylate (NSA), and covalently grafted it onto PDMS surfaces using UV irradiation. The ternary polymer coatings exhibited long-term stability in aqueous media and suppressed thenonspecific adsorption of proteins and cell adhesion. Furthermore, the immobilization of collagen on the side groups of NSA provides selective cell-adhesive functionality. In particular, PDMS surfaces modified with a ternary polymer containing 10 mol% NSA supported the robust and sustained adhesion of C2C12 myoblasts. When combined with stripe-patterned microstructures, these surfaces promoted unidirectional alignment, efficient myotube formation, and strong expression of dystrophin, with the 25 μm-pitch pattern demonstrating the most pronounced effects. Notably, spontaneous contraction of the formed myotubes confirmed advanced functional differentiation. These results demonstrate that the proposed facile and durable surface modification strategy for PDMS imparts both anti-biofouling properties and selective biofunctionality. The PDMS modification strategy provides a versatile platform for engineering functional muscle fibers and expanding the potential of PDMS-based bio-microdevices and tissue-engineered constructs.

1. Introduction

Among the attempts to reconstruct biological tissues *in vitro*, the most common approach remains the two-dimensional (2D) culture of cells on flat polystyrene substrates [1,2]. However, *in vivo* cells reside within a complex three-dimensional (3D) microenvironment in which mechanical and biochemical cues are tightly regulated. Therefore, 2D cultures fail to accurately recapitulate the *in vivo* environment, making it difficult to engineer physiologically relevant tissue constructs.

Alternatively, spheroid culture methods have also been used for *in vitro* tissue construction. Although these 3D cultures mimic certain aspects of the *in vivo* environment, they present challenges related to nutrient and oxygen diffusion, which limit the formation of large functional tissues. Another approach leverages tissue engineering techniques that combine microfabrication technologies and hydrogel engineering to create semi-3D or fully 3D culture environments [3–6].

Both the biochemical signals and mechanical cues from cellular scaffolds play critical roles in tissue regeneration [7,8]. Consequently, the development of optimal scaffold materials for cell culture–based tissue engineering has become a major area of investigation [9,10]. While many studies have focused on creating fully 3D scaffolds, increasing attention has been directed toward micropatterned 2D surfaces, often referred to as 2.5D culture systems, which offer spatial control over cell behavior [11,12].

* Corresponding authors.
E-mail addresses: nakaji@eng.u-toyama.ac.jp (T. Nakaji-Hirabayashi), YOSHIKAWA.Chiaki@nims.go.jp (C. Yoshikawa).

https://doi.org/10.1016/j.bbiosy.2025.100126
Received 28 October 2025; Received in revised form 14 December 2025; Accepted 29 December 2025
Available online 29 December 2025

Among the various candidate materials for tissue engineering scaffolds, polydimethylsiloxane (PDMS) has emerged as a promising substrate [5]. PDMS is a silicone-based elastomer that is known for its durability, flexibility, and ease of microfabrication. In addition, PDMS has excellent optical clarity, gas permeability, and chemical inertness toward biological materials, which has led to its increasing use in bioengineering applications. In clinical settings, PDMS is employed in devices such as catheters and contact lenses, whereas in research, it is widely used in microfluidic devices fabricated *via* bio-microfabrication techniques, including μTAS and MEMS, particularly in "lab-on-a-chip" technologies [13–17].

However, PDMS has several limitations. It is prone to nonspecific adsorption of biomolecules, and its native surface is not conducive to stable cell adhesion. Furthermore, because PDMS has a chemically inert surface with few reactive functional groups, surface modification is challenging [15]. Several methods for grafting polymers onto the PDMS surface have been proposed to overcome these issues, including oxygen plasma treatment, corona discharge, and vacuum UV irradiation. However, these techniques involve bond cleavage within the PDMS structure, thus resulting in only temporary surface modifications and limited long-term stability [18–20].

Our research group previously demonstrated that surfaces can be modified in a facile and stable manner using a photoreactive polymer containing *N*-benzophenone acrylamide (BPAm). Upon irradiation with UV light, BPAm can be covalently grafted onto hydrocarbon surfaces without requiring surface pretreatment [21]. Moreover, owing to its acrylamide backbone, the resulting polymer exhibits high resistance to hydrolysis and thus long-term surface stability [21]. Based on these findings, we hypothesized that this photoreactive polymer could be used to modify the surface of a PDMS substrate in a durable and facile manner.

In this study, we aimed to develop a stable cell-adhesive surface on PDMS by synthesizing a photo-crosslinkable copolymer that incorporates BPAm. To simultaneously suppress the nonspecific adsorption of biomolecules and provide selective cell-adhesive functionality, we designed a terpolymer composed of BPAm, *N*-(2-hydroxypropyl) acrylamide (HPAm), an antifouling monomer, and *N*-succinimidyl acrylate (NSA), which allows the conjugation of biofunctional molecules.

First, we demonstrate that our polymer provides a simple and stable long-term coating on PDMS surfaces. As a proof of concept for practical applications, we evaluated whether specific cell adhesion and functional cell differentiation could be achieved. In particular, collagen was conjugated to NSA residues and the surface was evaluated for its ability to support the adhesion and myogenic differentiation of C2C12 myoblasts, a model for muscle progenitor cells. Additionally, we used microfabrication, an inherent advantage of PDMS and a common technique in biofabrication, to create muscle-patterned PDMS substrates.

The simple and stable PDMS surface-modification technique developed in this study not only contributes to the advancement of bio-microfluidic devices and lab-on-a-chip systems, but also provides a technological foundation for constructing functional cell-based tissues on PDMS substrates. Such capabilities for the spatial control of cellular functions and long-term culture are expected to contribute to the future development of biomimetic tissue constructs, such as artificial muscles and skin.

2. Materials and methods

2.1. Synthesis of photo-crosslinkable polymers

The poly(HPAm-BPAm-NSA) copolymers were synthesized *via* free-radical polymerization using HPAm, BPAm, and NSA (Tokyo Chemical Industry, Tokyo, Japan) as ternary monomers (**Scheme S1**). HPAm and BPAm were synthesized according to a previously reported method [22]. The radical initiator 2,2′-azobisisobutyronitrile (AIBN; FUJIFILM Wako Pure Chemical, Osaka, Japan) was purified by recrystallization from ethanol prior to use.

In this study, three copolymers were synthesized by varying the molar ratio of NSA. The monomer feed ratios are listed in **Table S1**. The monomers and initiator were dissolved in dehydrated dimethylformamide (DMF), and dissolved oxygen was removed by purging with argon gas for 15 min. The polymerization was carried out at 70 °C for 2 h with stirring. The polymers were purified by precipitation in dehydrated acetone and collected as colorless powders after thorough drying in a vacuum desiccator. The synthesized poly(HPAm-BPAm-NSA) copolymers are denoted as PHBN*X*, where $X = 0$, 5, and 10 represents the molar percentage of NSA.

2.2. Characterization of photo-crosslinkable polymers

The compositional ratios of the synthesized polymers were determined using ^{1}H NMR spectroscopy (ECS-400, JEOL Ltd., Tokyo, Japan). The measurements were performed in dimethyl sulfoxide-d_6 (99.9 %) containing 1 vol % tetramethylsilane (TMS; FUJIFILM Wako Pure Chemical, Osaka, Japan) as the internal standard. The molecular weights of the polymers were determined using size-exclusion chromatography (HLC-8220, TOSOH, Tokyo, Japan) equipped with a Shodex LF-804 column (Resonac Holdings, Tokyo, Japan). The analysis was carried out at 40 °C with a flow rate of 0.8 mL/min, using DMF containing 10 mM LiCl as the mobile phase. Polystyrene standards (PStQuick, TOSOH) were used for calibration.

2.3. Preparation of polydimethylsiloxane sheets with/without stripes on the surface

A PDMS sheet with a flat surface was prepared. The SILPOT 184 Silicone Elastomer Base and Curing Agent (DuPont Toray Specialty Materials K.K., Tokyo, Japan) were mixed in a weight ratio of 10:1. The mixture (10 g) was poured into a polystyrene dish ($\varphi = 100$ mm) and degassed using a vacuum desiccator. After degassing, the mixture was allowed to cure on a level platform at 25 °C for 2 d. The cured PDMS sheets were cut into circular pieces ($\varphi = 14$ mm) using a round punch.

To fabricate PDMS sheets with striped micro-patterns, a micro-patterned plate (pitch height: 12 μm or 25 μm) was placed on a polystyrene dish ($\varphi = 100$ mm), and 10 g of the same PDMS mixture was poured onto it. Degassing and curing were performed under the aforementioned conditions. After curing, the patterned PDMS sheet was peeled off, the template was removed, and circular pieces ($\varphi = 14$ mm) were cut out using a round punch.

2.4. Surface modification of polydimethylsiloxane sheets with photo-crosslinkable polymers

The synthesized polymer was completely dissolved in a solvent mixture of dehydrated ethanol, dehydrated tetrahydrofuran, and dehydrated propanol in a volume ratio of 7:2:1 to prepare a 3 w/v % polymer solution. The PDMS sheet was washed alternately with ethanol and distilled water, followed by air drying with a nitrogen blower. The dried PDMS sheet was then placed on a spin coater (MS-A100, MIKASA, Tokyo, Japan), and 150 μL of the polymer solution was applied. The sheet was spin-coated at 3000 rpm for 60 s until the surface was evenly coated, whereupon the surface was irradiated with UV light (170 mW/cm^2; HB100A-1, AsOne, Osaka, Japan) for 3 min to induce crosslinking and surface modifications.

2.5. Collagen coating of polydimethylsiloxane surface modified with photo-crosslinkable polymers

The polymer-modified PDMS sheets were sterilized with 70 % ethanol and air-dried on a clean bench. The sheet was placed in a 24-well plate, immersed in 300 μL of collagen solution (TOYOBO, Osaka, Japan),

and incubated overnight at 37 °C in 5 % CO_2 to allow collagen immobilization *via* the NHS ester groups on the NSA side chains. After incubation, the sheet was washed thoroughly with Dulbecco's phosphate-buffered saline (PBS) to remove unreacted collagen.

For surface analysis, the sheet was washed with PBS, rinsed with distilled water, and air-dried prior to measurement. The samples modified with collagen are referred to as PHBN0-Col, PHBN5-Col, and PHBN10-Col.

For cell culture use, the washed sheet was immersed in growth medium (Dulbecco's Modified Eagle Medium–High Glucose (DMEM) supplemented with 10 % fetal bovine serum (FBS), 100 U/mL penicillin, and 100 μg/mL streptomycin) and stored under sterile conditions until cell seeding.

2.6. Characterization and analysis of polydimethylsiloxane surface

The thickness of the dried polymer-modified PDMS film was measured using a polarization-based film thickness measurement system (Automatic Ellipsometer MARY-102; Five Lab, Saitama, Japan). The measurement conditions were as follows: incident angle, 70°; light source, He–Ne laser (632.8 nm); refractive index of the bulk layer, 1.441; extinction coefficient, 0.035; and refractive index of the sample layer, 1.489, assuming a value similar to that of poly(methyl methacrylate) (PMMA) [23]. To assess the stability of the modified polymer, the film thickness was evaluated by comparing the samples immediately after polymer modification with those immersed in PBS for 2 weeks. X-ray photoelectron spectroscopy (XPS, ESCALAB 250Xi, Thermo Fisher Scientific K.K., Waltham, MA, USA) was used to analyze the surface elemental composition by recording the C 1s (280–300 eV), N 1s (392–410 eV), and Si 2p (95–110 eV) spectra. The measurement conditions were as follows: sample tilt angle, 0°; X-ray incident angle, 32.7°; detector reflection angle, 90°; and X-ray spot size, 650 μm.

To evaluate the wettability of the polymer-modified surfaces, water droplet and air bubble contact angles were measured using a contact angle meter (DMs-401, Kyowa Interface Science, Saitama, Japan). For the water droplet measurement, 1.0 μL of pure water was placed on the surface at room temperature, and the contact angle was measured after 30 s. For the air bubble measurement, a 1.0 μL air bubble was placed on the surface immersed in water, and the contact angle of the bubble was measured. The contact angle of each sample was measured 10 times and averaged.

2.7. Observation of polydimethylsiloxane surface using scanning electron microscopy

Various PDMS sheets were mounted on the sample stage and a compact sputtering system (QUICK COATER SC-701 MkII, Sanyu Electron, Tokyo, Japan) was used to deposit platinum (Pt) films onto the samples (5 mA, 30 s). Subsequently, the samples were mounted on a desktop scanning electron microscope (Miniscope TM4000PlusII, Hitachi High-Tech, Tokyo, Japan) and their surface morphologies were observed using a secondary electron detector at an acceleration voltage of 10 kV.

2.8. Assay for cells cultured on PDMS surfaces

2.8.1. Cell seeding and culture on substrates

The C2C12 mouse myoblast cell line (RIKEN BRC Cell Bank, Ibaraki, Japan) was cultured in a growth medium composed of DMEM supplemented with 10 % FBS and antibiotics until it reached a semi-confluent state. Adherent cells were detached using 0.05 % trypsin/ethylenediaminetetraacetic acid (EDTA) solution, suspended in growth medium, and collected as a cell pellets by centrifugation (500 × g, 15 °C, 5 min). After resuspension in growth medium, the cells were seeded onto various PDMS sheets and cultured at 37 °C in 5 % CO_2 atmosphere for the designated periods. Initial cell adhesion was evaluated by seeding the cells at a density of 3.0×10^4 cells/cm^2, after which they were cultured for 24 h. For long-term adhesion analysis, cells were seeded at a density of 2.0×10^3 cells/cm^2 and cultured for 2 weeks, with medium changes every 2 d.

To assess myotube and myofiber differentiation on various PDMS sheets, cells were seeded at a density of 3.0×10^4 cells/cm^2. For the microfabricated PDMS surfaces, the number of seeded cells was adjusted based on the actual surface area, considering the surface topography. After the cells were incubated in growth medium at 37 °C and 5 % CO_2 until reaching semi-confluence (~2 d), the cells were cultured in differentiation medium consisting of DMEM supplemented with 2 % horse serum and antibiotics for 1 week. The medium was changed every 2 d during the differentiation period.

2.8.2. Evaluation of adhesion and proliferation of cells cultured on a substrate

After culturing the cells on various PDMS sheets for either 24 h or 2 weeks, the samples were washed with PBS and fixed in 4 % paraformaldehyde (PFA) in PBS for 20 min to preserve the cellular structures. The cells were washed again with PBS to remove residual PFA, followed by treatment with 0.1 % Triton X-100 in PBS (Triton solution) for 20 min to permeabilize the cell membranes and facilitate antibody penetration. After another PBS wash, the cells were blocked with 1 % bovine serum albumin (BSA) in PBS for 30 min to preventnonspecific antibody binding. Subsequently, the cells were stained with Alexa Fluor 555 phalloidin (anti-actin, 1:100 dilution; Invitrogen) for 1 h to visualize actin filaments. After staining, the cells were thoroughly washed with PBS containing Tween-20 to remove unbound dye. Finally, the nuclei were counterstained using the ProLong Gold Antifade Reagent with DAPI (Invitrogen), and the adhesion state of the cells was observed using an inverted fluorescence microscope (DMIL-TR/EC3, Leica Microsystems, Tokyo, Japan).

2.8.3. Evaluation of differentiation of cells cultured on substrate

After 1 week of culturing in differentiation medium, the cells were fixed, permeabilized, and blocked following the procedures described previously. The cells were then stained using primary antibodies for the differentiation marker MyoD, which is expressed in myotube cells, and the structural protein dystrophin, which is selectively expressed in muscle fibers. The primary antibodies used were anti-MyoD (1:300; MyoD1 antibody; GeneTex, Kanagawa, Japan) and anti-dystrophin (1:300; dystrophin antibody [MANDRA1]; GeneTex), and the cells were incubated with these antibodies for 3 h. After thorough washing with PBS containing Tween-20, the cells were incubated with the following secondary antibodies: goat anti-rabbit IgG ($H + L$) cross-adsorbed Alexa Fluor 488 (1:500; Invitrogen, Waltham, MA, USA), goat anti-mouse IgG1 cross-adsorbed Alexa Fluor 594 (1:500; Invitrogen), and Hoechst 33,258 (1:500; Dojindo Laboratories, Kumamoto, Japan) for nuclear staining. Finally, the cells were thoroughly washed again with Tween solution and analyzed using an inverted fluorescence microscope (DMIL-TR/EC3; Leica Microsystems, Tokyo, Japan) to assess cell adhesion and differentiation status.

2.9. Gene expression analysis

To assess gene expression during myogenic differentiation, myoblasts were induced to differentiate into myotubes, and transcriptional profiles were analyzed at multiple time points using quantitative reverse transcription polymerase chain reaction (RT-qPCR). After complete removal of the culture medium, the cells were harvested using 0.25 % trypsin–1 mM EDTA solution and a cell scraper. Total RNA was extracted using the SV Total RNA Isolation System (Promega, Madison, WI, USA) and quantified using a spectrophotometer (ND-2000, Thermo Fisher Scientific, Waltham, MA, USA). The extracted RNA was reverse transcribed using ReverTra Ace qPCR RT Master Mix with gDNA Remover (TOYOBO, Osaka, Japan) to synthesize complementary DNA (cDNA).

RT-qPCR was performed using the synthesized cDNA as a template with KOD SYBR qPCR Mix (TOYOBO).

Primers and probes targeting glyceraldehyde 3-phosphate dehydrogenase (GAPDH, housekeeping gene), MyoD, Myogenin, and dystrophin were used (**Table S2** [37,38]). The relative gene expression levels were evaluated using the ΔΔCT method.

2.10. Statistical analysis

The water and bubble droplet contact angles, cell adhesion, and gene expression results were statistically analyzed using JMP software (JMP Pro 15, SAS Institute, Tokyo, Japan). One-way analysis of variance was used to evaluate statistical significance. For multiple comparisons, Tukey's honest significant difference test was used. A p-value of less than 0.05 was considered statistically $p < 0.05$.

3. Results

3.1. Characteristics of photocrosslinkable polymers and polymer-modified PDMS sheets

The comonomer compositions of the synthesized polymers were analyzed by ^{1}H NMR spectroscopy (**Fig. S1**). The compositions of PHBN0, PHBN5, and PHBN10 were 97:3, 93:3:4, and 88:3:9, respectively, which are in good agreement with the corresponding monomer feed ratios. The number-average molecular weight (M_n) and weight-average molecular weight (M_w) of each copolymer were evaluated using gel permeation chromatography (GPC) (Table S3). All polymers exhibited Mw values exceeding 3.0×10^5, and no clear differences were observed among the copolymers with different feed compositions. The thicknesses of the polymer layers formed on the PDMS were measured immediately after surface modification and also after incubation in PBS for two weeks (Table 1). The initial coating thicknesses of PHBN0, PHBN5, and PHBN10 were approximately 230 nm, and comparable thicknesses were maintained after immersion in PBS, although a slight increase in variation was detected.

The chemical structures of the polymer-modified PDMS surfaces were characterized with the aid of X-ray photoelectron spectroscopy (XPS) (Fig. 1**A**). The C 1s spectra of these surfaces, compared with that of unmodified PDMS, exhibited an intensification of the C–C peak at 284 eV and the appearance of a C=O peak at 287 eV. The N 1s spectrum was characterized by a peak at 398 eV, attributable to the C–N bonds, which appeared after the polymer modification. The Si 2p spectra exhibited marked decreases in the intensities of the peaks originating from the siloxane backbone of the unmodified PDMS, Si–C (99.8 eV), and Si–O (102 eV).

The wettability of these surfaces was evaluated by measuring the contact angles of water droplets and air bubbles (Fig. 1**B,C**). In addition, the water contact angle of each of the modified surfaces was measured after incubation in PBS for two weeks (**Fig. S2**). Compared with the unmodified PDMS, the polymer-modified PDMS surfaces had lower water contact angles and higher air-bubble contact angles. After collagen treatment, the water contact angle further decreased and the air-bubble contact angle increased in PHBN5 and PHBN10, whereas almost no change was observed for PHBN0. In comparison, the water contact angle of the unmodified PDMS changed by a small amount, whereas the air-bubble contact angle increased. The water contact angles measured after immersion in PBS were similar to those measured before immersion, and the hydrophobic recovery of the polymer-modified surfaces was insignificant.

Table 1
Thickness of photo-crosslinkable polymer modified on PDMS surface.

Polymer	Thickness (nm)	
	Before incubation in PBS	After incubation in PBS for 2 weeks*
PHBN0	238 ± 1.4	241 ± 4.0
PHBN5	235 ± 1.5	224 ± 7.7
PHBN10	233 ± 1.6	234 ± 2.2

* Polymer-coated PDMS sheets were immersed in PBS at 37 °C for two weeks to assess the durability of the coating polymer.

3.2. Adhesion of myoblasts on polymer-modified PDMS surfaces

Representative images of cells cultured for 24 h on each polymer-modified surface are shown in Fig. 2**A**. The results of the quantitative analysis to determine the number of adherent cells are shown in Fig. 2**B**, and the results for the collagen-treated surfaces after two weeks of culture are shown in Fig. 2**C**. Almost no adherent cells were observed on the unmodified PDMS. In contrast, PDMS-Col, which was immersed in a collagen solution, supported cell adhesion comparable to that observed in conventional tissue culture polystyrene dishes. All collagen-free PHBN0, PHBN5, and PHBN10 surfaces exhibited low cell adhesion. However, after collagen treatment, cell adhesion and spreading on PHBN5-Col and PHBN10-Col markedly increased, with PHBN10-Col exhibiting a higher cell density than PHBN5-Col. Furthermore, PHBN5-Col and PHBN10-Col maintained cell adhesion even after 2 weeks of culture, whereas unmodified PDMS did not.

3.3. Adhesion of myoblasts on stripe-micropatterned PDMS surfaces

Cross-sectional SEM images of PDMS substrates fabricated with stripe micropatterns (groove widths of 12 μm and 25 μm) (Fig. 3**A**) confirmed that the replicated structures accurately corresponded with the dimensions of the original mold. The plan-view SEM images further demonstrate that the striped patterns were uniformly transferred onto the PDMS surfaces.

Each PDMS substrate with a stripe micropattern was coated with PHBN10-Col, after which SEM images of the adherent cells were acquired. Many cells adhered to the groove regions of the striped structures and aligned and elongated along the groove direction. A comparison of the 12 μm and 25 μm stripe-micropatterned PDMS substrates revealed that cells on the former exhibited a very slender, highly elongated morphology along the grooves, whereas on the latter, a similar elongation tendency was observed but with many cells stacked and aggregated within the grooves as they extended.

3.4. Myotube formation on polymer-modified PDMS substrates

Myoblasts were cultured to confluence on PHBN10-Col–modified stripe-micropatterned PDMS surfaces and flat PDMS surfaces and then induced to differentiate into myotubes for 7 d. The extent of differentiation was evaluated using immunostaining and RT-qPCR (Fig. 3**B,C**). For immunostaining, the muscle-specific markers MyoD and dystrophin were analyzed, and for RT-qPCR, the expression levels of MyoD, Myogenin, and dystrophin were quantified.

On day 3 of differentiation, the cells cultured on polystyrene dishes (PS) and flat PDMS exhibited elongated fibrous morphologies extending in various directions. By days 5 and 7, the number of fibrous cells increased and the fibers became thicker. Immunofluorescence images confirmed the expression of dystrophin, and multiple nuclei (blue) were observed within individual fibers. In contrast, on stripe-micropatterned PDMS surfaces modified with PHBN10-Col, cells adhered to and spread along the microgroove patterns. By day 5 of differentiation, many cells had assembled into fiber-like structures, and by day 7, most cells had developed into fiber bundles, a phenomenon particularly pronounced on the 25 μm-pitch PDMS surface. Immunostaining revealed a strong expression of MyoD and dystrophin, which were localized in multinucleated cells.

The fusion behavior of myoblasts was evaluated quantitatively by calculating the fusion index as the percentage of nuclei located within dystrophin-positive myotubes relative to the total number of nuclei

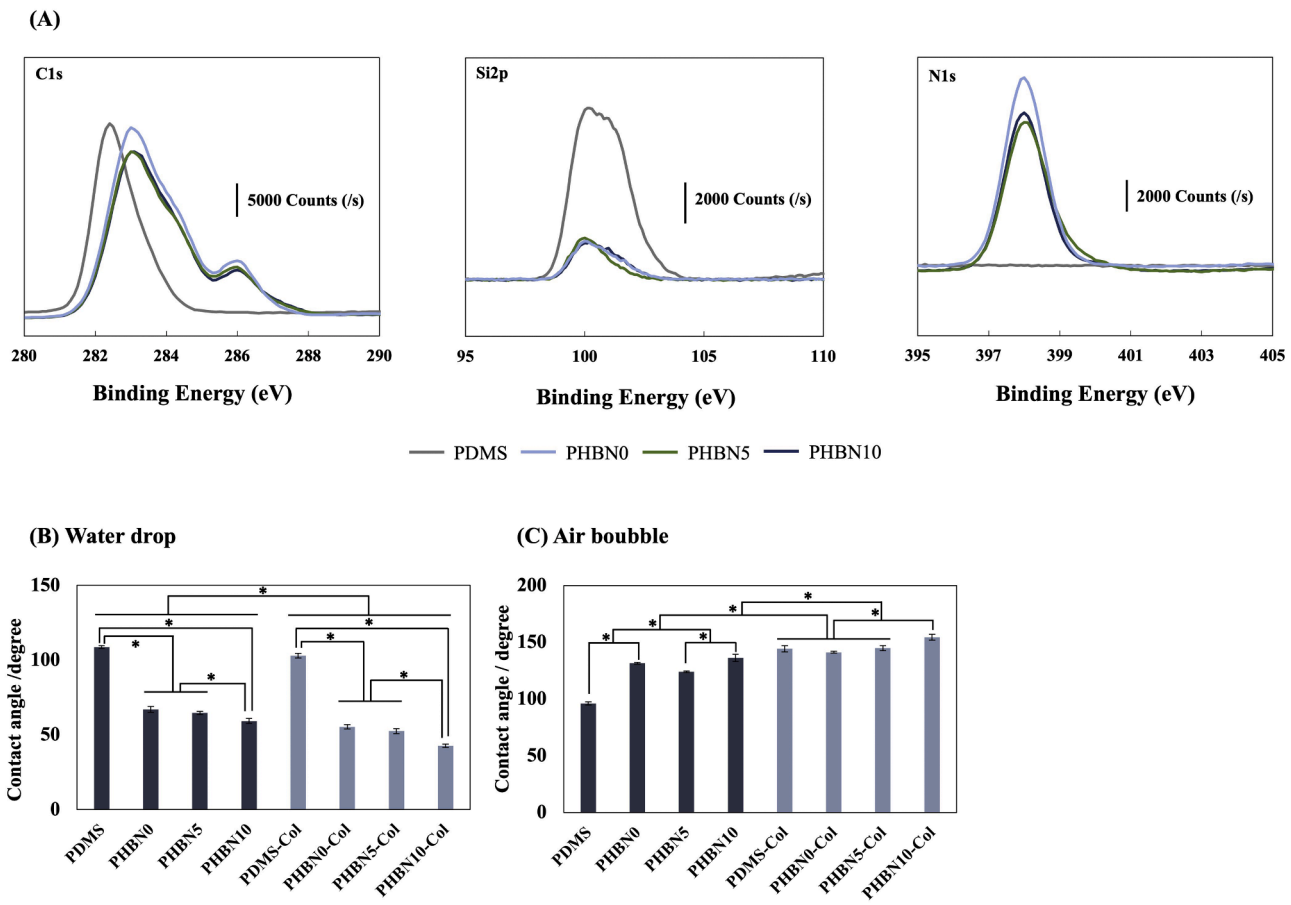

Fig. 1. Surface characterization of unmodified and PHBN-coated PDMS. (A) XPS results (C 1s, N 1s, and Si 2p) of unmodified and modified (with PHBN) PDMS surfaces. (B) Water droplet contact angles and (C) air bubble contact angles of unmodified and polymer-modified PDMS (PHBN0, PHBN5, and PHBN10), before and after incubation in collagen solution (PDMS-Col, PHBN0-Col, PHBN5-Col, and PHBN10-Col). *Indicates statistical significance ($n = 3$, $p < 0.05$). These results indicate that the PHBN coatings uniformly cover the PDMS surface, increase its hydrophilicity, and enable composition-dependent collagen immobilization.

(**Fig. S4**). The fusion indices on PS and flat PDMS were approximately 30 % and 40 %, respectively, whereas those on the 12 μm and 25 μm stripe-micropatterned PDMS surfaces were both as high as 75–80 %, indicating that the micropatterned PDMS surfaces substantially promoted myoblast fusion.

RT-qPCR analysis revealed a stepwise expression profile from the early to middle stages of differentiation. MyoD expression was high at the early stage, followed by an increase in myogenin expression, and finally, an upregulation of dystrophin expression at a later stage (**Fig. S3**). No substantial differences in the expression levels of MyoD or Myogenin were observed between the different surface topographies. In contrast, dystrophin expression was significantly increased on the 25 μm PDMS surface, reaching levels that were approximately two-fold higher than on the flat PDMS surface and about 1.5-fold higher than on the 12 μm PDMS surface. Furthermore, as additional evidence supporting the maturation of myotubes, spontaneous contractile activity was observed in cells cultured on the 25 μm PDMS surface (**Video 1**).

4. Discussion

Polydimethylsiloxane (PDMS) has been widely used in biomedical devices because of its excellent flexibility, processability, optical transparency, and oxygen permeability [24]. However, its high hydrophobicity often results innonspecific protein adsorption and heterogeneous cell adhesion. Apart from this, most existing surface modification methods are disadvantaged by insufficient long-term stability, which limits their use as reliable cell culture substrates [25,26]. To overcome these issues, we established a new surface design that integrated three functions: chemical immobilization, suppression of nonspecific adsorption, and introduction of specific cell-adhesive ligands. In particular, we designed and synthesized a photo-crosslinkable terpolymer (PHBN) composed of three functional units: BPAm, HPAm, and NSA. Furthermore, taking advantage of the intrinsic suitability of PDMS for microfabrication, we fabricated substrates with microscale striped patterns. By combining selective cell adhesion mediated by the PHBN with cell alignment induced by microtopography, we aimed to promote myotube formation on PDMS substrates.

The stability of PHBN films also needs to be considered. According to many reports, polymer coatings on PDMS are prone to surface disruption owing to delamination, hydrolysis, and swelling. In contrast, in this study, the thickness of the PHBN films remained essentially unchanged, even after immersion in PBS for two weeks. This suggests that both the strong covalent immobilization via BPAm and high hydrolytic stability derived from the acrylamide backbone contribute to the robustness of the coating.

The XPS profiles clearly display distinct peaks corresponding to the C–C, C=O, and C–N bonds originating from the polymer, whereas the contributions from the Si–C and Si–O bonds, which are characteristic of unmodified PDMS, were markedly reduced. These spectral changes indicate that the polymer films were widely spread across the PDMS surface. The slight residual Si 2p signal is likely attributable to local fluctuations in the film thickness or to very small uncovered regions, considering the information depth of XPS (approximately 2-4 nm).

With respect to changes in the surface hydrophilicity, modification of the PHBN polymer markedly decreased the water contact angle of the PDMS surface. Given that the water contact angle of HPAm

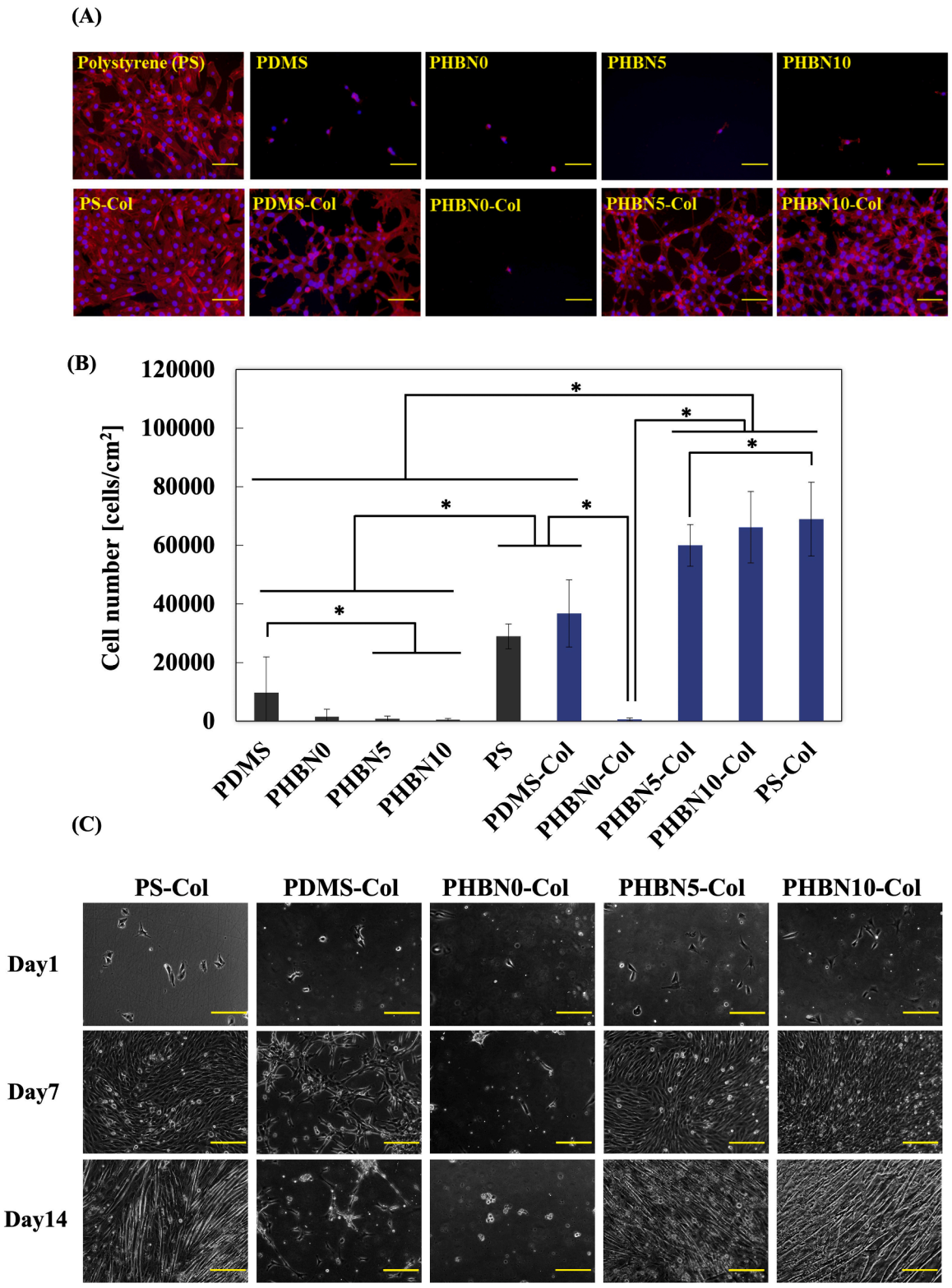

Fig. 2. Cell adhesion and long-term culture of C2C12 myoblasts on PHBN-modified PDMS surfaces. (A) Immunofluorescence images of cells cultured for 24 h on polystyrene, unmodified PDMS, and PDMS surfaces modified with PHBN0, PHBN5, and PHBN10. All surfaces were either left unincubated (upper panels) or incubated with collagen solution (lower panels). F-actin (red) and nuclei (blue) of adhered cells were stained with phalloidin and DAPI, respectively. Scale bars: 200 μm. (B) Number of adhered cells after 24 h of culture on unmodified PDMS and PDMS surfaces modified with PHBN0, PHBN5, and PHBN10. All surfaces were either unincubated (dark gray bars) or incubated (blue bars) with collagen solution. * Indicates statistical significance ($n = 3$, $p < 0.05$). (C) Phase-contrast images of cells cultured for two weeks on polystyrene, unmodified PDMS, and PDMS surfaces modified with PHBN0, PHBN5, and PHBN10. All surfaces were incubated with collagen solution. Scale bars: 200 μm. These results demonstrate that PHBN0 effectively suppressed nonspecific cell adhesion, whereas collagen-immobilized PHBN10 supported selective and long-term cell adhesion on PDMS substrates.

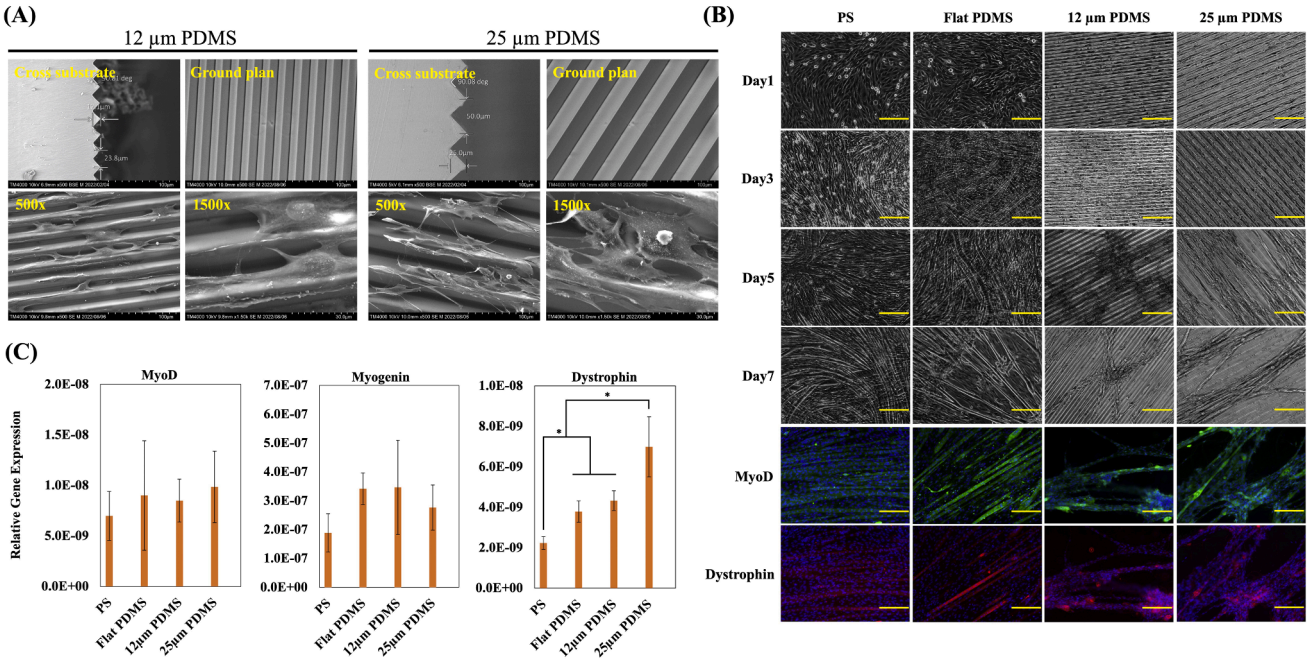

Fig. 3. Effect of stripe micropatterning on alignment and myogenic differentiation of C2C12 myoblasts on PHBN10-Col–modified PDMS. (A) SEM images of stripe-micropatterned PDMS substrates (upper panels) and C2C12 cells adhered to PHBN10-Col–modified stripe-micropatterned PDMS (lower panels). Left: PDMS substrate with 12 μm-deep stripe micropattern; right: PDMS substrate with 25 μm-deep stripe micropattern. (B) Phase-contrast and immunofluorescence images of cells adhered to PHBN10-Col–modified stripe-micropatterned PDMS. MyoD (green), dystrophin (red), nuclei (blue). Scale bar: 200 μm. (C) Relative gene expression levels of MyoD, Myogenin, and dystrophin in cells after 7 d of differentiation into myotubes on each substrate, normalized to GAPDH expression in each sample. * Indicates statistical significance ($n = 3$, $p < 0.05$). These results demonstrate that PHBN10-Col–modified stripe micropatterns, particularly with a depth of 25 μm, promote aligned myotube formation and enhance myogenic maturation.

homopolymer has been reported to be 44 ± 3° [27], the enhanced hydrophilicity observed in this study can be ascribed to the presence of the HPAm units. Furthermore, in PHBN5 and PHBN10, the introduction of collagen via NSA groups led to a further increase in surface hydrophilicity [28–30]. In contrast, PHBN0 does not have NSA groups and, therefore, cannot form covalent bonds with collagen, resulting in only limited changes in the contact angle. Because PDMS is intrinsically hydrophobic, it readily permits nonspecific physical adsorption of proteins; however, in the case of PHBN0, HPAm-derived bioinertness suppresses protein adsorption. Therefore, unlike bare PDMS, PHBN0 is less likely to physically adsorb collagen, which explains why the surface properties remained largely unaffected.

Cell adhesion assays were performed on surface-modified PDMS substrates to evaluate the performance of the developed photocrosslinkable polymers. On unmodified PDMS, proteins in the culture medium are physically adsorbed onto the highly hydrophobic surface, allowing cells to adhere transiently. However, this physically adsorbed protein layer was unstable, and with increasing culture time, the proteins gradually desorbed, leading to detachment of the cells. On PDMS-Col, which was immersed in collagen solution, cell adhesion comparable to that on tissue culture polystyrene dishes was initially observed. This behavior was attributed to the physical adsorption of collagen onto the PDMS surface; nevertheless, the cells on PDMS-Col gradually detached as the culture period became longer. These observations are consistent with previous reports, indicating that although PDMS is an attractive material from a mechanical and processing standpoint, it is unsuitable as a substrate for long-term cell culture [26], and they reaffirm the difficulty of establishing a stable, durable, cell-adhesive environment on PDMS surfaces.

In contrast, on surfaces covered with PHBN0, which contains HPAm units in the backbone, nonspecific protein adsorption was strongly suppressed, and nonspecific cell adhesion, as observed on unmodified PDMS, did not occur. Even on the PHBN0-Col surfaces subjected to collagen treatment, cell adhesion remained inhibited, indicating that PHBN0 exhibited a pronounced HPAm-derived bioinert characteristic. For PHBN5 and PHBN10, which contain NSA groups, collagen could be covalently immobilized; thus, these surfaces exhibited bioinert behavior similar to that of PHBN0 in the absence of collagen treatment, whereas after collagen treatment, stable cell adhesion and cell spreading were observed. In particular, PHBN10 contained a greater number of NSA groups, allowing a larger amount of collagen to be immobilized, thereby supporting a higher cell density than that of PHBN5. Moreover, after two weeks of culture, the cells remained stably attached without any sign of cell detachment, in contrast to the behavior on PDMS-Col. These findings indicate that collagen immobilization via NSA forms a durable cell-adhesive layer, in contrast to the instability of physically adsorbed coatings.

Taken together, these results demonstrate that the PHBN polymers developed in this study enable the construction of PDMS surfaces that exhibit the long-term suppression of nonspecific biointeractions, a property that is difficult to achieve using conventional approaches. In addition, surface modification with PHBN5 and PHBN10 allowed the selective induction of cell adhesion and provided a stable cell culture environment over extended periods. Although collagen was used as the model adhesive protein in this study, similar effects could be expected when other extracellular matrix (ECM) proteins are used. Therefore, surface modification strategies based on PHBN polymers are considered highly versatile for a wide range of biological applications.

The alignment and behavior of myoblasts on the microstructured PDMS surfaces were found to depend strongly on the groove width and depth. All cell-based evaluations on the micropatterned substrates were performed using PDMS modified with PHBN10-Col, which demonstrated the highest cell-adhesive performance and long-term stability in the preceding adhesion assays. This modification ensures a homogeneous cell-adhesive environment, allowing the sole influence of microtopography on cellular responses to be appropriately evaluated.

On flat PDMS surfaces, the expression of MyoD and dystrophin was detected; however, many cells remained mononuclear, and a large proportion of the population corresponded to immature cells at an intermediate stage of differentiation. By contrast, on the micropatterned surfaces, most cells became multinucleated and formed clearly identifiable fiber bundles, indicating that the microstructures strongly promoted myoblast fusion and myotube formation. Notably, the effectiveness of microstructural cues was highly dependent on the groove depth. On the 12 μm pattern, cells initially spread along the grooves at the early adhesion stage; however, as fusion progressed, the resulting cell bundles frequently bridged across adjacent grooves and expanded laterally to ultimately form fiber bundles with random orientation. This behavior suggests that the 12 μm groove depth is effectively shallow for cells and insufficient to confine the fused cell assemblies. In other words, although the 12 μm grooves contributed to initial directional guidance, they failed to maintain structural confinement once cell fusion advanced, thus leading to a loss of long-range alignment.

In contrast, on the 25 μm pattern, cells remained stably attached within the grooves and formed highly unidirectional muscle fiber bundles. The groove depth of 25 μm appears to provide sufficient confinement for both migrating cells and fused multinuclear assemblies. This confinement prevents them from escaping from the grooves and thereby preserving alignment even after fusion. In the differentiation experiments, the 25 μm pattern exhibited the strongest myotube-forming capability. The expression level of dystrophin was approximately 2-fold higher than that on flat PDMS and about 1.5-fold higher than that on the 12 μm pattern, indicating a marked enhancement of myotube maturation. Furthermore, the observation of spontaneous contractile activity under these conditions supports not only the morphological but also the functional maturation of myotubes.

In this study, we quantitatively evaluated the amount of newly deposited cell-derived ECM on PHBN-modified PDMS substrates. However, because collagen is pre-immobilized on the surface as an adhesive ligand, it is technically difficult to selectively assess the cell-derived ECM components. ECM deposition and remodeling are widely known to influence myogenic differentiation and tissue maturation. Therefore, a more detailed analysis of the ECM network formed on PHBN-modified PDMS remains an important subject for future investigation.

The surface modification based on photo-crosslinking employed in this study has several technical limitations. First, the coating uniformity in immobilization with the aid of UV irradiation, may be compromised by non-uniform illumination and shadowing effects caused by the substrate geometry. In this study, uniform UV irradiation was applied to flat PDMS substrates and those with simple stripe patterns. Membrane thickness measurements, XPS results, and contact angle analyses confirmed that these surface properties were consistent and that a homogeneous polymer coating was formed on these flat geometries. However, extension of this approach to three-dimensional structures or substrates with complex internal architectures, where light penetration is restricted, necessitates optimization of the irradiation conditions, including the incident angle, spatial light intensity distribution, and intrinsic optical transparency of PDMS.

Second, the potential effects of UV exposure on the substrate must be considered in UV-based immobilization. Although PDMS is relatively stable under UV irradiation, prolonged exposure or irradiation at shorter wavelengths could induce surface hardening or minor chain-scission events [31,32]. For applications involving cell culture or high-performance functional substrates, it is necessary to optimize irradiation conditions and systematically evaluate possible substrate degradation.

Considering these technical aspects, the comparison of PHBN polymer coatings with existing PDMS modification strategies highlights several important distinctions. Oxygen plasma and corona discharge treatments can transiently increase the surface hydrophilicity; however, hydrophobic recovery caused by the reorientation of the Si–O–Si backbone is essentially unavoidable, resulting in a rapid loss of the surface modification effect [26,33]. Surface modification with PEG or self-assembled monolayers (SAMs) is effective for suppressing nonspecific adsorption; however, the resulting layers are typically very thin and prone to delamination due to mechanical abrasion or hydrolysis [34–36]. In contrast, the PHBN polymers developed in this study uniquely offer, within a single process, (1) robust covalent immobilization via BPAm, (2) mechanical stability derived from coatings with thicknesses exceeding 200 nm, (3) high bioinertness imparted by HPAm, and (4) selective introduction of ECM proteins through NSA groups. Moreover, the synthesis was accomplished in a single step via radical polymerization and did not require specialized equipment, providing practical advantages in terms of cost and operational simplicity.

Collectively, these features indicate that PHBN polymer coatings represent a promising approach to overcome the inherent limitations of conventional PDMS modification methods, namely the “lack of long-term stability” and the “difficulty in maintaining surface functionality.” Thus, this coating strategy can be considered a highly applicable and practical surface modification technique for PDMS-based devices.

5. Conclusion

In this study, a ternary copolymer composed of HPAm as a bioinert monomer, BPAm as a photocrosslinkable monomer, and NSA as a collagen-binding unit was synthesized and used to modify PDMS surfaces via UV irradiation. The modified PDMS surfaces were characterized by film thickness measurements, XPS analysis, and contact angle measurements to evaluate their surface properties. The results demonstrated the formation of relatively thick polymer films ($\geq$200 nm), which remained stable without significant change, even after immersion in water for two weeks. Furthermore, the observed decrease in the water contact angle and increase in the bubble contact angle on the collagen-treated surfaces indicated successful collagen immobilization *via* the NSA moieties. Cell adhesion studies using myoblasts revealed that the PHBN0-modified surfaces exhibited bioinert properties, whereas cell adhesion on the PHBN5-Col and PHBN10-Col surfaces was comparable to that of polystyrene. These findings were consistent even after two weeks of culture, confirming the stability of the bioinert and cell-adhesive surfaces. Based on these results, PHBN10 was employed as a surface-modifying agent on two types of microstructured PDMS substrates for myoblast-to-myotube differentiation experiments. Dystrophin expression was observed on all tested surfaces, indicating enhanced myogenic differentiation. In particular, myoblasts cultured on the 25 μm micro-patterned PDMS surfaces, which promoted unidirectional alignment, enabled efficient differentiation into myotubes and spontaneous beating. These findings demonstrate that the synthesized HPAm/BPAm/NSA copolymer enables the facile and stable surface modification of PDMS to create bioinert yet cell-adhesive surfaces. Although collagen was used as the adhesive ligand in this study, substitution with other matrix proteins allowed for selective cell adhesion, highlighting the versatility of this surface modification platform. Furthermore, the spontaneous beating of myotubes observed on the micropatterned PDMS indicated that the combination of polymer-based surface modification and microtopographical guidance enabled the construction of functional muscle fibers on PDMS substrates.

Data availability statement

All data supporting the findings of this study are available in the article and Supplementary Information files.

CRediT authorship contribution statement

Ryoma Takagi: Writing – original draft, Visualization, Validation, Methodology, Investigation, Formal analysis, Data curation. **Tadashi Nakaji-Hirabayashi:** Writing – review & editing, Supervision, Project

administration, Funding acquisition, Conceptualization. **Moe Kato:** Validation, Methodology, Investigation, Formal analysis, Data curation. **Miwako Shobo:** Validation, Investigation, Formal analysis, Data curation. **Chiaki Yoshikawa:** Writing – review & editing, Supervision, Project administration, Methodology, Funding acquisition, Conceptualization.

Declaration of competing interest

The authors declare that they have no known competing financial interests or personal relationships that could have appeared to influence the work reported in this paper.

Acknowledgments

This study was supported by Grants-in-Aid (17KK01130, 18K19907, 22H03951, T. Nakaji-Hirabayashi) and (19KK0368, 22H02133, C. Yoshikawa) from the Ministry of Education, Culture, Sports, Science, and Technology (MEXT), Tokyo, Japan; the Hisaharu AME Charitable Research Foundation, Toyama, Japan; an Academic Research Grant from the Yamaguchi Educational and Scholarship Foundation; and a HOKURIKU BANK Grant-in-Aid for Young Scientists. Additional support was provided by the Joint Research Hub Program of the National Institute for Materials Science (NIMS) and JST SPRING (Grant Number JPMJSP2145). The authors are also grateful to Editage for English language editing.

Supplementary materials

Supplementary material associated with this article can be found, in the online version, at doi:10.1016/j.bbiosy.2025.100126.

References

[1] Becker J, Blanchard K. Characterization of primary breast carcinomas grown in three-dimensional cultures. J Surg Res 2007;142:256–62. https://doi.org/10.1016/j.jss.2007.03.016.
[2] Ferreira L, Gaspar V, Mano J. Design of spherically structured 3D *in vitro* tumor models -Advances and prospects. Acta Biomater 2018;75:11–34. https://doi.org/10.1016/j.actbio.2018.05.034.
[3] Thangadurai M, Ajith A, Budharaju H, Sethuraman S, Sundaramurthi D. Advances in electrospinning and 3D bioprinting strategies to enhance functional regeneration of skeletal muscle tissue. Biomater Adv 2022;142:213135. https://doi.org/10.1016/j.bioadv.2022.213135.
[4] Pina S, Ribeiro V, Marques C, Maia F, Silva T, Reis R, Oliveira J. Scaffolding Strategies for Tissue Engineering and Regenerative Medicine Applications. Materials (Basel) 2019;12:1824. https://doi.org/10.3390/ma12111824.
[5] Tenje M, Cantoni F, Hernández A, Searle S, Johansson S, Barbe L, Antfolk M, Pohlit H. A practical guide to microfabrication and patterning of hydrogels for biomimetic cell culture scaffolds. Organ- Chip 2020;2:100003. https://doi.org/10.1016/j.ooc.2020.100003.
[6] Jana S, Levengood S, Zhang M. Anisotropic materials for skeletal-muscle-tissue engineering. Adv Mater 2016;28:10588–612. https://doi.org/10.1002/adma.201600240.
[7] Yamazawa Y, Kato H, Nakaji-Hirabayashi T, Yoshikawa C, Kitano H, Ohno K, Saruwatari Y, Matsuoka K. Bioinactive semi-interpenetrating network gel layers: zwitterionic polymer chains incorporated in a cross-linked polymer brush. J Mater Chem B 2019;7:4280–91. https://doi.org/10.1039/c8tb03228a.
[8] Place E, Evans N, Stevens M. Complexity in biomaterials for tissue engineering. Nat Mater 2009;8:457–70. https://doi.org/10.1038/nmat2441.
[9] Egawa E, Kato K, Hiraoka M, Nakaji-Hirabayashi T, Iwata H. Enhanced proliferation of neural stem cells in a collagen hydrogel incorporating engineered epidermal growth factor. Biomater 2011;32:4737–43. https://doi.org/10.1016/j.biomaterials.2011.03.033.
[10] Kloxin A, Kasko A, Salinas C, Anseth K. Photodegradable hydrogels for dynamic tuning of physical and chemical properties. Science (1979) 2009;324:59–63. https://doi.org/10.1126/science.1169494.
[11] Qazi T, Mooney D, Pumberger M, Geissler S, Duda G. Biomaterials based strategies for skeletal muscle tissue engineering: existing technologies and future trends. Biomater 2015;53:502–21. https://doi.org/10.1016/j.biomaterials.2015.02.110.
[12] Yang H, Ieronimakis N, Tsui J, Kim H, Suh K, Reyes M, Kim D. Nanopatterned muscle cell patches for enhanced myogenesis and dystrophin expression in a mouse model of muscular dystrophy. Biomater 2014;35(5):1478–86. https://doi.org/10.1016/j.biomaterials.2013.10.067.
[13] Dardouri M, Aljnadi I, Deuermeier J, Santos C, Costa F, Martin V, Fernandes M, Gonçalves L, Bettencourt A, Gomes P, Ribeiro I. Bonding antimicrobial rhamnolipids onto medical grade PDMS: a strategy to overcome multispecies vascular catheter-related infections. Colloids Surf B 2022;217:112679. https://doi.org/10.1016/j.colsurfb.2022.112679.
[14] Lin C, Yeh Y, Lin W, Yang M. Novel silicone hydrogel based on PDMS and PEGMA for contact lens application. Colloids Surf B 2014;123:986–94. https://doi.org/10.1016/j.colsurfb.2014.10.053.
[15] Jo M, Guldiken R. Effects of polydimethylsiloxane (PDMS) microchannels on surface acoustic wave-based microfluidic devices. Microelectron Eng 2014;113:98–104. https://doi.org/10.1016/j.mee.2013.07.021.
[16] Bonyár A, Santha H, Ring B, Varga M, Kovács J, Harsányi G. 3D rapid prototyping technology (RPT) as a powerful tool in microfluidic development. Procedia Eng 2010;5:291–4. https://doi.org/10.1016/j.proeng.2010.09.105.
[17] Becker H, Gärtner C. Polymer microfabrication technologies for microfluidic systems. Anal Bioanal Chem 2008;390(1):89–111. https://doi.org/10.1007/s00216-007-1692-2.
[18] Tan S, Nguyen N, Chua Y, Kang T. Oxygen plasma treatment for reducing hydrophobicity of a sealed polydimethylsiloxane microchannel. Biomicrofluidics 2010;4:032204. https://doi.org/10.1063/1.3466882.
[19] Hillborg H, Gedde U. Hydrophobicity recovery of polydimethylsiloxane after exposure to corona discharges. Polymer (Guildf) 1998;39(10):1991–8. https://doi.org/10.1016/s0032-3861(97)00484-9.
[20] Efimenko K, Wallace W, Genzer J. Surface modification of Sylgard-184 poly (dimethyl siloxane) networks by ultraviolet and ultraviolet/ozone treatment. J Coll Int Sci 2002;254(2):306–15. https://doi.org/10.1006/jcis.2002.8594.
[21] Yoshikawa C, Takagi R, Nakaji-Hirabayashi T, Ochi T, Kawamura Y, Thissen H. Marine antifouling coatings based on durable bottlebrush polymers. ACS Appl Mater Interfaces 2022;14:32497–509. https://doi.org/10.1021/acsami.2c06647.
[22] Yoshikawa C, Nakaji-Hirabayashi T, Nishijima N, Nonsuwan P, Toh R, Kowalczyk W, Thissen H. Ultra-low fouling photocrosslinked coatings for the selective capture of cells expressing CD44. Mater Sci Eng C 2021;120:111630. https://doi.org/10.1016/j.msec.2020.111630.
[23] Li B, Pan S, Yuan H, Zhang Y. Optical and mechanical anisotropies of aligned electrospun nanofibers reinforced transparent PMMA nanocomposites. Compos Part A Appl Sci Manuf 2016;90:380–9. https://doi.org/10.1016/j.compositesa.2016.07.024.
[24] Fujii T. PDMS-based microfluidic devices for biomedical applications. Microelectron Eng 2002;61:907–14. https://doi.org/10.1016/s0167-9317(02)00494-x.
[25] Pérez-Calixto M, Peto-Gutiérrez C, Shapiro A, Huerta L, Hautefeuille M, Macías-Silva M, Pérez-Calixto D, Vázquez-Victorio G. Enhanced PDMS functionalization for organ-on-a-chip platforms using ozone and sulfo-SANPAH: a simple approach for biomimetic long-term cell cultures. Adv Healthc Mater 2025;14:13. https://doi.org/10.1002/adhm.202404686.
[26] Chuah Y, Heng Z, Tan J, Tay L, Lim C, Kang Y, Wang D. Surface modifications to polydimethylsiloxane substrate for stabilizing prolonged bone marrow stromal cell culture. Colloids Surf B Biointerfaces 2020;191:110995. https://doi.org/10.1016/j.colsurfb.2020.110995.
[27] Fairbanks B, Thissen H, Maurdev G, Pasic P, White J, Meagher L. Inhibition of protein and cell attachment on materials generated from N-(2-hydroxypropyl) acrylamide. Biomacromolecules 2014;15(9):3259–66. https://doi.org/10.1021/bm500654q.
[28] Sofi H, Abdal-hay A, Rashid R, Rafiq A, Rather S, Beigh M, Alrokayan S, Khan H, Tripathi R, Sheikh F. Electrospun polyurethane fiber mats coated with fish collagen layer to improve cellular affinity for skin repair. SM&T 2022;34:e00523. https://doi.org/10.1016/j.susmat.2022.e00523.
[29] Sharma D, Jia W, Long F, Pati S, Chen Q, Qyang Y, Lee B, Choi C, Zhao F. Polydopamine and collagen coated micro-grated polydimethylsiloxane for human mesenchymal stem cell culture. Bioact Mater 2019;4:142–50. https://doi.org/10.1016/j.bioactmat.2019.02.002.
[30] Zichen Q, David R, Wenkai J, Qi X, Feng Z. Bioactive polydimethylsiloxane surface for optimal human mesenchymal stem cell sheet culture. Bioact Mater 2018;3(2):167–73. https://doi.org/10.1016/j.bioactmat.2018.01.005.
[31] Wang Z, Qian L, Peng X, Huang Z, Yang Y, He C, Fang P. New aspects of degradation in silicone rubber under UVA and UVB irradiation: a gas chromatography–mass spectrometry study. Polymers (Basel) 2021;13. https://doi.org/10.3390/polym13132215.
[32] Efimenko K, Wallace W, Genzer J. Surface modification of Sylgard-184 poly (dimethyl siloxane) networks by ultraviolet and ultraviolet/ozone treatment. J Colloid Interface Sci 2002;254(2):306–15. https://doi.org/10.1006/jcis.2002.8594.
[33] Feng C, Li Y, Luo Y, Zhang L, Zong Y, Zhao K. Mechanisms of hydrophobic recovery of poly(dimethylsiloxane) elastomers after plasma/corona treatments: a minireview. Langmuir 2024;40:45. https://doi.org/10.1021/acs.langmuir.4c03086.
[34] Zhang Z, Wang J, Tu Q, Nie N, Sha J, Liu W, Liu R, Zhang Y, Wang J. Surface modification of PDMS by surface-initiated atom transfer radical polymerization of water-soluble dendronized PEG methacrylate. Colloids Surf B Biointerfaces 2011;88(1):85–92. https://doi.org/10.1016/j.colsurfb.2011.06.019.
[35] Sui G, Wang J, Lee C, Lu W, Lee S, Leyton J, Wu A, Tseng H. Solution-phase surface modification in intact poly(dimethylsiloxane) microfluidic channels. Anal Chem 2006;78(15):5543–51. https://doi.org/10.1021/ac060605z.

[36] Song Y, Feng A, Liu Z, Li D. Zeta potentials of PDMS surfaces modified with poly (ethylene glycol) by physisorption. Electrophoresis 2020;41. https://doi.org/10.1002/elps.201900246.
[37] Garcia J, Panitch A, Calve S. Functionalization of hyaluronic acid hydrogels with ECM-derived peptides to control myoblast behavior. Acta Biomater 2019;84:169–79. https://doi.org/10.1016/j.actbio.2018.11.030.
[38] Hildyard J, Wells D. Identification and validation of quantitative PCR reference genes suitable for normalizing expression in normal and dystrophic cell culture models of myogenesis. PLoS Curr 2014;6. https://doi.org/10.1371/currents.md.faafdde4bea8df4aa7d06cd5553119a6.